The Planetary Science Journal, 7:201 (16pp), 2026 August https://doi.org/10.3847/PSJ/ae8ba4

Constraints on Magma Self-oxidation in Angrites and the Role of Parent-body Size

Hideharu Kuwahara[1,3], Damanveer S. Grewal[2,3], and Kyusei Tsuno[2]
[1] Geodynamics Research Center, Premier Institute for Advanced Studies (PIAS), Ehime University, Ehime, Japan; kuwahara.hideharu.vd@ehime-u.ac.jp
[2] Department of Earth and Planetary Sciences, Yale University, New Haven, CT, USA; damanveer.grewal@yale.edu
Received 2026 February 26; revised 2026 June 29; accepted 2026 July 12; published 2026 August 19

Abstract

Earth, and potentially Venus, formed through giant impacts involving early-formed planetesimals and planetary embryos in the inner solar system, but the size distribution of these bodies remains poorly constrained. Angrites sample one of the earliest differentiated bodies in the inner solar system and preserve a marked redox contrast with HEDs: evolved angrites record oxygen fugacity (fO_2) near-iron-wüstite (IW) or slightly supra-IW conditions, whereas HEDs are ∼1–2 log units more reduced. This difference has been interpreted to indicate a comparatively oxidized mantle for an angrite parent body (APB), but most fO_2 estimates are derived from evolved magmas that may not track deep-mantle conditions. Here, we explore whether internal magma self-oxidation driven by Fe^{3+} stabilization in a deep magma ocean followed by fractional crystallization can account for the redox state of evolved angrites and what this implies for APB size. We combine parameterizations of $Fe^{3+}/\Sigma Fe$ in silicate melts with fractional crystallization models of Group 1–2 angrites, starting from metal-saturated conditions consistent with primitive angrites. We find that magma self-oxidation reproduces the fO_2 inferred for evolved angrites only if core–mantle equilibration pressures exceed several gigapascals. Such pressures imply a body substantially larger than asteroid Vesta. For plausible APB compositions and starting redox states, radii of ∼1250–2500 km are required, comparable to or exceeding the size of the Moon and overlapping independent geobarometric estimates. Rather than uniquely determining APB size, our results provide a redox-based lower bound on its size and demonstrate that internal oxidation offers a viable mechanism for generating oxidized signatures in evolved angrites.

Unified Astronomy Thesaurus concepts: Planetesimals (1259); Planetary science (1255); Planet formation (1241); Achondrites (15); Mantle (1005)

1. Introduction

Earth, and potentially Venus, are thought to have formed via giant impacts involving planetesimals and Moon- to Mars-sized planetary embryos (J. M. Chambers & G. W. Wetherill 1998; R. M. Canup & E. Asphaug 2001; A. N. Halliday & R. M. Canup 2023). Identifying the presence of such embryos, and characterizing their chemical compositions, in the early inner solar system is therefore critical to understand the formation of terrestrial planets. However, direct geochemical fingerprints of these bodies in terrestrial planets, particularly Earth, remain elusive because energetic giant impacts and subsequent vigorous mantle convection erased their original chemical signatures after accretion.

Achondrites, such as angrites and Howardites–Eucrites–Diogenites (HEDs, likely from asteroid Vesta; R. P. Binzel & S. Xu 1993), sample the silicate portions of the earliest differentiated rocky bodies in the inner solar system, providing key constraints on the nascent stages of terrestrial planet formation. Although the angrite parent body (APB) has not been identified, estimates of its size have ranged from a Vesta-sized body (i.e., 260 km in radius) (B. P. Weiss et al. 2008; E. R. Scott & W. F. Bottke 2011; K. Keil 2012) to 1085–1405 km in radius (F. L. H. Tissot et al. 2022), and ⩾1000 km from clinopyroxene geobarometry (A. S. Bell et al. 2026), approaching the Moon (i.e., 1740 km in radius). Magma oceans in their parent bodies are inferred from their homogeneous oxygen isotopic compositions (i.e., $\Delta^{17}O$) (R. C. Greenwood et al. 2005), while rapid core segregation in magma-ocean environments is inferred from their Hf/W chronometry (T. Kleine et al. 2004; 2012; R. C. Greenwood et al. 2005; A. Markowski et al. 2007; M. Touboul et al. 2015) and depletion of refractory siderophile elements (e.g., Ni and Co) (K. Righter & M. J. Drake 1997; K. Righter 2008). Despite these similarities indicating that both Vesta and APB had metal-saturated reducing silicate mantles, these two groups of meteorites display a striking dichotomy in their oxygen fugacity (fO_2) (A. J. G. Jurewicz et al. 1993; M. Wadhwa 2008).

1.1. fO_2 Dichotomy between Angrites and HEDs

The fO_2 of Vesta's mantle, inferred from HEDs, is 1 log-unit below the iron-wüstite (IW) buffer (ΔIW−1) (A. J. G. Jurewicz et al. 1993; M. Wadhwa 2008), consistent with metal-silicate equilibration in a magma-ocean environment (i.e., ΔIW−2) (E. S. Steenstra et al. 2016). In contrast, redox-sensitive geochemical indicators, such as Eu/Gd partitioning in plagioclase and pyroxene, suggest that plutonic angrites (e.g., LEW 86010, NWA 2999, NWA 4590, and NWA 4801) crystallized from magmas with fO_2 near ΔIW +1 ± 1 (G. McKay et al. 1994; M. E. Sanborn & M. Wadhwa 2021). However, these estimates based on Eu/Gd partitioning between plagioclase-clinopyroxene pairs are inherently tied to the final stages of crystallization and therefore may only reflect evolved magmatic conditions rather than the primitive mantle redox state. Experimental studies

[3] These authors contributed equally.

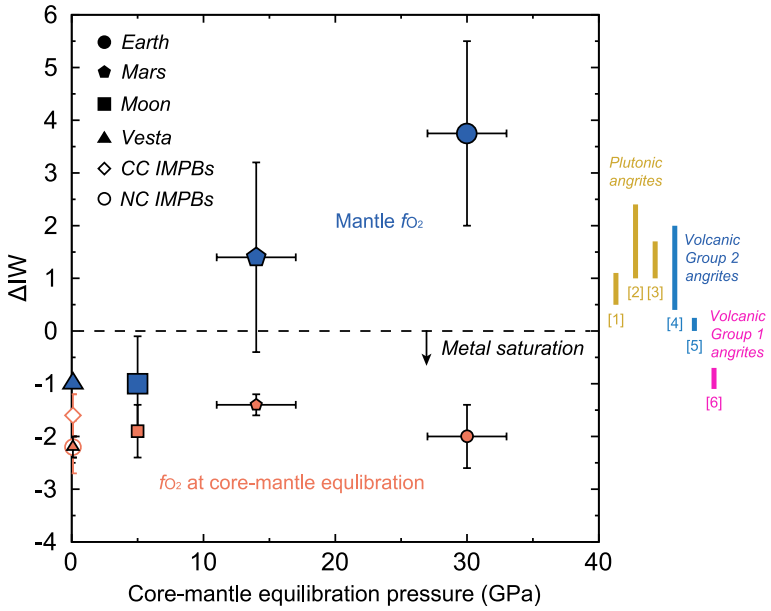

Figure 1. fO_2 during core formation and in present-day mantles of rocky bodies. fO_2 is shown as the log-unit difference relative to the IW buffer. Blue and orange symbols represent present-day mantle fO_2 values and fO_2 during magma-ocean stages associated with core–mantle equilibration, respectively. Core–mantle equilibration pressures and magma-ocean fO_2 data are from E. S. Steenstra et al. (2016, 2017), D. S. Grewal et al. (2022a, 2024), M. M. Hirschmann (2022), N. Rai & W. van Westrenen (2014), K. Righter & N. L. Chabot (2011), and K. Righter (2011). Present-day mantle fO_2 data are from D. J. Frost et al. (2008) and references therein, R. W. Nicklas et al. (2021), and H. Zhang et al. (2024b). Yellow, blue, and pink vertical bars indicate estimated fO_2 ranges for plutonic angrites [1] NWA 2999, [2] NWA 4590, and [3] NWA 4801 (M. E. Sanborn & M. Wadhwa 2021), volcanic Group 2 angrites [4] D'Orbigny (F. L. H. Tissot et al. 2022) and [5] D'Orbigny, Sahara 99555, and NWA 12004 (A. S. Bell et al. 2023a), and volcanic Group 1 angrite [6] NWA 12774 (A. S. Bell et al. 2023b).

based on high Mg# of clinopyroxene in volcanic angrites (D'Orbigny and NWA 1296) also yield comparable redox estimates (F. L. H. Tissot et al. 2022). Moreover, Fe^{3+}-bearing ulvöspinel in these angrites supports their formation under relatively oxidizing conditions (K. Keil 2012 and references therein). However, trace amounts of Fe, Ni metals found in some volcanic angrites (e.g., LEW 87051, NWA 1670, and Sahara 99555) have been linked to their formation under reducing conditions close to metal saturation (K. Keil 2012 and references therein), suggesting that better constraints on magma fO_2 in angrite lithology are needed.

A recent petrological study has classified volcanic angrites into two main groups: magnesian-rich volcanic angrites (Mg# = molar Mg/(Mg + Fe) = 55–60), such as LEW 87051, NWA 1670, and NWA 12774 (hereafter referred to as Group 1), and less magnesian volcanic angrites (Mg# 30–35), such as D'Orbigny, Sahara 99555, and NWA 1296 (hereafter referred to as Group 2) (F. L. H. Tissot et al. 2022). Group 2 angrites were likely produced by fractional crystallization of primitive Group 1 magmas (F. L. H. Tissot et al. 2022). To constrain fO_2 of evolved Group 2 angrite magmas, A. S. Bell et al. (2023a) developed a new oxybarometer in the olivine–spinel–silicate liquid assemblages and suggested that the magmatic fO_2 of volcanic angrites (Sahara 99555, D'Orbigny, and NWA 12004) was more reducing than previously estimated (i.e., ΔIW+0 to +0.25). Although the newly estimated fO_2 of volcanic angrites are closer to those expected for a metal-saturated magma-ocean environment, they are still 1.5–2 log units higher than those expected for Vesta's and APB magma oceans (E. S. Steenstra et al. 2016; 2017), implying magma oxidation during the final stages of crystallization (A. S. Bell et al. 2023a). In contrast, the Cr valence state of olivine cores and thermodynamic modeling of primitive Group 1 angrites, such as NWA 12774, suggests that their mantle sources equilibrated at IW–0.9 ± 0.2 (A. S. Bell et al. 2023b), pointing to a reduced, metal-saturated deep interior.

Experimental studies show that clinopyroxene saturation in Group 2 angrites occurs only after ∼50% crystallization (S. J. McKibbin & H. S. C. P. O'Neill 2018; F. L. H. Tissot et al. 2022), implying that most existing fO_2 estimates for Group 2 angrites—derived from late-stage assemblages such as Eu/Gd partitioning in plagioclase-clinopyroxene pairs or olivine–spinel–liquid equilibria—primarily reflect shallow, evolved magmas rather than primitive mantle melts. Evolved liquids are also susceptible to auto-oxidation and degassing, further decoupling their fO_2 from that of the deep mantle (A. S. Bell et al. 2023a). Therefore, existing fO_2 constraints on Group 2 angrites should be treated as shallow magmatic endpoints and not direct measures of the bulk mantle redox state. Notably, such a pronounced mantle-to-surface fO_2 gradient (based on Group 1 and Group 2 angrites, respectively) (Figure 1 and Table 1) has not been documented for other small rocky bodies, including Vesta. This redox stratification—from a reduced, metal-saturated deep interior to more oxidized shallow magmatic systems—appears to be a distinctive feature of the APB, but the mechanism responsible for this evolution remains debated. Below, we evaluate two candidate mechanisms: postcore formation water-induced oxidation (Section 1.2) and internally driven magma self-oxidation (Section 1.3).

1.2. Limited Effect of Water-induced Magma Oxidation

The fO_2 of evolved Group 2 angrites appears inconsistent with metal-silicate equilibration in a magma-ocean environment (K. Righter & M. J. Drake 1997; K. Righter 2008; E. S. Steenstra et al. 2016; 2017). Reconciling this discrepancy requires an oxidation mechanism in a shallower part of APB during a postcore formation and/or late-stage crystallization of

Table 1
Estimated fO_2 of Angrites

	ΔIW	Error	References
Plutonic angrites			
LEW 86010[a]	∼0.8	…	G. McKay et al. (1994)
NWA 2999[a]	0.8	0.3	M. E. Sanborn & M. Wadhwa (2021)
NWA 4590[a]	1.7	0.7	M. E. Sanborn & M. Wadhwa (2021)
NWA 4801[a]	1.35	0.35	M. E. Sanborn & M. Wadhwa (2021)
Volcanic group 2 angrites			
D'Orbigny[b]	1.2	0.8	F. L. H. Tissot et al. (2022)
D'Orbigny, Sahara 99555, NWA 12004[c]	0.125	0.125	A. S. Bell et al. (2023a)
Volcanic group 1 angrites			
NWA 12774[d]	−0.9	0.2	A. S. Bell et al. (2023b)

Notes.
[a] fO_2 estimated from Eu/Gd partitioning between plagioclase and clinopyroxene cores.
[b] fO_2 estimated from the Mg# (molar Mg/(Mg + Fe) ratio) of pyroxene cores.
[c] fO_2 estimated using the olivine-spinel-$a^{liq}_{SiO_2}$ oxybarometer, where $a^{liq}_{SiO_2}$ denotes the silica activity in the liquid.
[d] fO_2 estimated from the Cr valence state in olivine cores.

angrite magmas. Water, a major oxidant in early solar system materials (C. M. Q'D. Alexander 2019; D. S. Grewal et al. 2024), could have elevated mantle fO_2 after core formation. Although angrites derive from the noncarbonaceous (NC; inner solar system) reservoir (I. J. Onyett et al. 2023) and are highly depleted in volatile elements, particularly alkalis (K. Keil 2012; F. A. J. Abernethy et al. 2013; 2018), this does not imply accretion from entirely dry materials. Studies of NC magmatic iron meteorites (samples of the earliest planetesimal cores) indicate that inner solar system planetesimals initially accreted MVE-enriched, water-, carbon-, and nitrogen-bearing materials (D. S. Grewal et al. 2021a, 2022a, 2024, 2025a; D. S. Grewal & P. D. Asimow 2023; D. S. Grewal & S. Mukhopadhyay 2025). Vesicles in some angrite basalts further support residual volatiles in the APB mantle (T. J. McCoy et al. 2006). If water persisted after core formation, water–rock reactions such as $2FeO + H_2O = Fe_2O_3 + H_2$ could have converted ferrous to ferric iron, releasing H_2 and raising mantle fO_2. Such reactions provide a plausible mechanism for postcore oxidation of the APB mantle.

Evaluating water-induced postcore formation mantle oxidation on the APB requires constraining the relative timing of core formation and volatile-loss events. If the APB underwent extensive volatile loss before or during the core formation, as has been proposed for several early inner solar objects, including the parent bodies of NC and CC iron meteorites, as well as primitive and differentiated achondrites from both reservoirs (R. R. Fu & L. T. Elkins-Tanton 2014; D. S. Grewal et al. 2021b, 2022b, 2024, 2025c; D. S. Grewal 2022; M. E. Newcombe et al. 2023; L. D. Peterson et al. 2023a, 2023b), then substantial postcore formation oxidation of the mantle by water would not have been possible. Instead, metal-silicate equilibration during core formation would likely have maintained the redox state of the mantle below the IW buffer, as observed in HEDs (A. J. G. Jurewicz et al. 1993; M. Wadhwa 2008) and NC iron meteorites (D. S. Grewal et al. 2024; 2025b). This suggests that the APB mantle was volatile-depleted, and therefore likely dry, at the time of core formation.

Alternatively, the observed difference in fO_2 between Group 2 angrites and HEDs could reflect varying levels of late accretion, with APB experiencing a greater influx of oxidizing, water-bearing materials, consistent with its higher fO_2. Using Os concentrations of $\sim 1\,ng\,g^{-1}$ in the APB mantle (C. W. Dale et al. 2012) and $\sim 500\,ng\,g^{-1}$ in CI chondrites (J. T. Wasson & G. W. Kallemeyn 1988), we estimate that ∼0.2 wt% CC materials would have been incorporated into the APB mantle. Given that water-rich CC materials (e.g., CI and CM chondrites) can contain up to ∼10 wt% H_2O (A. Morbidelli et al. 2012 and references therein), this corresponds to a delivery of $\sim 200\,\mu g\,g^{-1}$ of H_2O to the APB mantle during late accretion. While this value is broadly comparable to independent estimates of H_2O content in the APB mantle derived from the less degassed olivine and pyroxene in plutonic angrite NWA 4801 ($85–110\,\mu g\,g^{-1}$; B. G. Rider-Stokes et al. 2024a), the D/H ratios of NWA 4801 suggest a carbonaceous chondrite-like indigenous water source rather than late accretion (B. G. Rider-Stokes et al. 2024a). The Os-based estimate therefore provides an upper bound on water delivery via late accretion, and the actual contribution may have been substantially lower.

However, the plausible range of H_2O contents in the APB mantle is insufficient to account for the Fe_2O_3 content inferred from the fO_2 of Group 2 angrites. The averaged FeO content in Group 2 angrites has been estimated to be 24.40 wt% (F. L. H. Tissot et al. 2022). To explain fO_2 of evolved Group 2 angrites (ΔIW >0) (A. S. Bell et al. 2023a) at the melting conditions (i.e., 0.6–0.9 GPa) (F. L. H. Tissot et al. 2022), ∼1.08 wt% of Fe_2O_3 equivalent to ∼0.04 of $Fe^{3+}/\Sigma Fe$ ratios are needed. To quantify the maximum redox effect of H_2O in the magma, we assume that all H_2O is used to oxidize Fe^{2+} to Fe^{3+}. The amount of Fe_2O_3 generated by the H_2O-induced oxidation was calculated as

$$C^{Mantle}_{Fe_2O_3}(\text{Oxidation}) = \frac{C^{Mantle}_{H_2O} M_{Fe_2O_3}}{M_{H_2O}} \quad (1)$$

where $C^{Mantle}_{Fe_2O_3}$ and $C^{Mantle}_{H_2O}$ are the mass concentrations of Fe_2O_3 and H_2O in the APB mantle, and $M_{Fe_2O_3}$, and M_{H_2O} are their respective molecular weights. Within the plausible range of H_2O: $85–110\,\mu g\,g^{-1}$ (B. G. Rider-Stokes et al. 2024a) and our estimates on late delivery ($\sim 200\,\mu g\,g^{-1}$), Equation (1) yields only negligible amounts of Fe_2O_3 (0.08–0.18 wt%), which are insufficient to account for the Fe_2O_3 content (∼1.08 wt%) inferred from the fO_2 of Group 2 angrites.

The limited oxidative role of H_2O is also supported by mineralogical evidence. Olivine and clinopyroxene from volcanic (e.g., Asuka 12209) and plutonic angrites (e.g., NWA 4801) contain $<10\,\mu g\,g^{-1}$ H_2O (B. G. Rider-Stokes et al. 2024a), indistinguishable from eucritic clinopyroxenes ($\sim 4–11\,\mu g\,g^{-1}$) (A. R. Sarafian et al. 2019). Despite similar water contents, angrites record higher fO_2 than eucrites, which formed well below the IW buffer. Thus, redox differences between APB and Vesta cannot be explained by water content alone. Considering Vesta's reducing mantle (∼IW–1) (A. J. G. Jurewicz et al. 1993; M. Wadhwa 2008) and the dryness of the APB mantle, late-accreted materials likely had little effect on mantle oxidation. Therefore, exogenous sources alone are unlikely to account for the elevated fO_2 in evolved

Group 2 angrites; while residual water-related reactions may have contributed somewhat alongside other processes (see Section 4.5), an internally driven oxidation process is required as the dominant mechanism.

1.3. Internally Driven Magma Self-oxidation

Alternatively, the elevated fO_2 in evolved Group 2 angrites may reflect an endogenous oxidation mechanism. One candidate is the charge disproportionation of ferrous iron (Fe^{2+}) to ferric iron (Fe^{3+}) and metallic iron (Fe^0) within a deep magma ocean, where Fe^0 sinks into the core, enriching the mantle in ferric iron and raising its fO_2 (M. M. Hirschmann 2012; K. Armstrong et al. 2019; J. Deng et al. 2020; H. Kuwahara et al. 2023; H. L. Zhang et al. 2024a). Experimental and theoretical work confirm that Fe^{2+} in silicate melt can disproportionate into Fe^{3+} and Fe^0 (metal) at pressures exceeding ~5 GPa (K. Armstrong et al. 2019; J. Deng et al. 2020; H. Kuwahara et al. 2023; H. L. Zhang et al. 2024a). Structural changes in Fe-O bonding in compressed basaltic glass further support this mechanism; Fe^{3+}–O coordination increases earlier than Fe^{2+}–O at pressures up to 15 GPa, indicating that Fe^{3+} becomes more stable than Fe^{2+} at depth due to its smaller partial molar volume (K. Ozawa et al. 2022). Additionally, natural evidence of high-pressure Fe^{2+} disproportionation has been reported in lunar impact glass formed by micrometeorite impacts (C. Li et al. 2022; H. Xian et al. 2023; Z. Cao et al. 2024). Some angrites (Asuka 12209, Asuka 881371, and NWA 12320) contain impact-generated melts, as indicated by the differences in oxygen isotopic compositions between olivine xenocrysts and the surrounding groundmass (B. G. Rider-Stokes et al. 2023), and Fe^{3+} stabilization in such impact melts may be possible. However, most other volcanic angrites show no evidence of exogenous contamination or shock metamorphism (K. Keil 2012), suggesting that the fO_2 of these volcanic angrites is not modified after the eruption and preserves the fO_2 of the magma. Collectively, these findings indicate that Fe^{2+} disproportionation in a deep magma ocean, followed by segregation of disproportionated metal (Fe^0) into the core, can significantly increase a rocky body's intrinsic fO_2, as long as core–mantle equilibration occurred at pressures >5 GPa.

An important point to emphasize is the positive relationship between mantle fO_2 and core–mantle equilibration pressure (CMEP) (or parent-body size) across differentiated rocky bodies (Figure 1) (see also Tables A1, A2). Bodies with shallow core–mantle boundaries—i.e., iron meteorite parent bodies (IMPBs), Vesta, and the Moon—, despite their significant difference in size, exhibit similarly low mantle fO_2 values, which lie well below the IW buffer (M. Wadhwa 2008; D. S. Grewal et al. 2024). In contrast, larger differentiated bodies such as Mars and Earth have mantle fO_2 values that are ~3–6 orders of magnitude more oxidizing than would be predicted from metal-silicate equilibration alone. This relationship supports the hypothesis that magma self-oxidation is associated with deep metal-silicate equilibration.

Magma fO_2 could also increase during crystallization when Fe^{3+} is incompatible with minerals more than Fe^{2+}. Indeed, basaltic samples derived from Vesta and the Moon show 0.5–1 log units higher fO_2 than those estimated for magma oceans (Figure 1), suggesting internally driven magma oxidation during crystallization. Because Group 2 angrites were likely produced by fractional crystallization of primitive Group 1 magmas (F. L. H. Tissot et al. 2022), these two groups provide an important opportunity to examine the effects of internal magma-oxidation processes. Here, we estimate $Fe^{3+}/\Sigma Fe$ ratio and fO_2 of Group 1 and 2 angrite magmas by considering the effects of high-pressure stabilization of Fe^{3+} during metal-silicate equilibration and subsequent fractional crystallization. Taking these considerations together with recent geochemical constraints on the fO_2 of angrites, we investigate the permitted size range of APB based on a magma self-oxidation model (without external oxidant addition). Our approach is novel in two respects: first, we explicitly combine the pressure-dependent $Fe^{3+}/\Sigma Fe$ parameterization with a fractional crystallization model specific to the angrite crystallization sequence, providing a quantitative framework for testing whether self-oxidation alone can bridge the gap between the reduced Group 1 and more oxidized Group 2 magmas; second, by benchmarking the model against both Vesta and the Moon, we demonstrate the internal consistency of the approach before applying it to the APB.

2. Methods

2.1. Initial Conditions of the APB Magma Ocean

We adopt initial magma-ocean fO_2 values in the range ΔIW–1.4 ± 0.5, consistent with estimates for metal-saturated core–mantle equilibration (E. S. Steenstra et al. 2017) and with the reduced fO_2 of primitive Group 1 angrites, such as NWA 12774 (IW–0.9 ± 0.2 at 1.5–1.8 GPa; A. S. Bell et al. 2023b; A. S. Bell et al. 2026). We then evaluate whether Fe^{3+} stabilization in a deep magma ocean, followed by fractional crystallization, can generate evolved melts with fO_2 comparable to the IW+0–0.25 range inferred for diabasic and evolved Group 2 angrites (A. S. Bell et al. 2023a).

To estimate the $Fe^{3+}/\Sigma Fe$ ratio of Group 1 angrites, we assume that their $Fe^{3+}/\Sigma Fe$ ratios approximate that of the magma ocean established at a given CMEP. This assumption is motivated by two considerations. First, the melting phase equilibria of NWA 1670 and LEW 87051 indicate olivine-orthopyroxene multiple saturation near the liquidus at pressures of ~2–3 GPa, suggesting equilibration with a lherzolitic mantle assemblage (F. L. H. Tissot et al. 2022) and implying that these Group 1 angrites represent melts generated by relatively high degrees of partial melting in the APB mantle. Second, although Group 1 angrites may have experienced some degree of fractional crystallization, the effect of olivine crystallization on the $Fe^{3+}/\Sigma Fe$ ratio of the residual melts is expected to be limited. In particular, Group 1 angrites contain relatively high amounts of Cr_2O_3 (0.14–0.45 wt%) (NWA 1670, LEW 87051, and NWA 12774) compared to Group 2 angrites (~0.04 wt%) (F. L. H. Tissot et al. 2022 and references therein; Y. He et al. 2024), which may compensate the increased $Fe^{3+}/\Sigma Fe$ ratios of the residual melts during crystallization through redox exchange reaction $2CrO + Fe_2O_3 = Cr_2O_3 + 2FeO$ (M. M. Hirschmann 2022). More specifically, 0.14–0.45 wt% of Cr_2O_3 could reduce 0.007–0.022 of $Fe^{3+}/\Sigma Fe$ ratios in magma assuming the averaged FeO content in Group 1 angrites (i.e., 19.09 wt%) (F. L. H. Tissot et al. 2022). The close agreement in fO_2 between the inferred magma ocean (E. S. Steenstra et al. 2017) and Cr-rich NWA 12774 (ΔIW–0.9 ± 0.2; A. S. Bell et al. 2023b; Cr_2O_3 = 0.3–0.45 wt%; Y. He et al. 2024) supports the view that fractional crystallization had a limited effect on the $Fe^{3+}/\Sigma Fe$ ratio of Group 1 angrites from the APB mantle.

2.2. Estimation of the $Fe^{3+}/\Sigma Fe$ Ratio of APB Magma Ocean

The $Fe^{3+}/\Sigma Fe$ ratio of the APB magma ocean was calculated at a given pressure and intermediate solidus-liquidus temperature of KLB-1 peridotite (D. C. Rubie et al. 2015 and references therein) using the thermodynamic model of C. Sun & L. Yao (2024) which comprehensively compiled previous experimental data. Here, we consider the relative stability of Fe^{3+} to Fe^{2+} in the magma ocean using the oxygen exchange reaction

$$FeO + \frac{1}{4}O_2 = FeO_{1.5}. \quad (2)$$

In this case, the $Fe^{3+}/\Sigma Fe$ ratio of the magma ocean at a given fO_2, pressure, and temperature is described using the Gibbs free energy of the reaction (2)

$$\ln\left(\frac{X_{FeO_{1.5}}}{X_{FeO}}\right) = \frac{1}{4}\ln f_{O_2} - \ln\left(\frac{\gamma_{FeO_{1.5}}}{\gamma_{FeO}}\right) - \frac{\Delta G(T,\ P_0)}{RT} - \int_{P_0}^{P}\frac{\Delta V}{RT}dP. \quad (3)$$

Here, $X_{FeO_{1.5}}$, X_{FeO}, $\gamma_{FeO_{1.5}}$, and γ_{FeO} are mole fractions and activity coefficients of $FeO_{1.5}$ (Fe^{3+}) and FeO (Fe^{2+}), respectively. $\Delta G(T,\ P_0)$ is the Gibbs free energy of the reaction (2) at 1 bar. ΔV is the change in the volume of the reaction (2). R, T, and P are the ideal gas constant, temperature, and pressure, respectively. Based on Equation (3), the effects of temperature, pressure, and magma compositions on $Fe^{3+}/\Sigma Fe$ ratio of the magma have been estimated (K. Armstrong et al. 2019; J. Deng et al. 2020; M. M. Hirschmann 2022; H. Kuwahara et al. 2023; C. Sun & L. Yao 2024; H. L. Zhang et al. 2024a). In this study, we used the model of Fe^{2+} disproportionation in magma under high pressure and temperature by C. Sun & L. Yao (2024). The authors compiled comprehensive previous experimental data ($n = 1069$) for a wide range of fO_2 (ΔIW–2 to +14), pressure (1 bar to 24 GPa), temperature (1073–2873 K), and composition (e.g., 0–79 wt% of SiO_2; 0.6–92 wt% of FeO_{total}). Their model yields the smallest residuals between predicted and experimentally determined fO_2 values compared to other available parameterizations (K. Armstrong et al. 2019; J. Deng et al. 2020; M. M. Hirschmann 2022; H. Kuwahara et al. 2023; H. L. Zhang et al. 2024a), particularly at low-SiO_2 melts (<40 wt%), which is appropriate for Group 1 and 2 angrite magmas (i.e., 39.14–41.16 wt%; F. L. H. Tissot et al. 2022 and references therein). It is also noted that all experimental and theoretical studies (K. Armstrong et al. 2019; J. Deng et al. 2020; M. M. Hirschmann 2022; H. Kuwahara et al. 2023; H. L. Zhang et al. 2024a) have shown the positive pressure dependence of $Fe^{3+}/\Sigma Fe$ ratios at a given fO_2 at pressures above ~5 GPa. Thus, while the quantitative estimates of CMEPs are model-dependent, the qualitative conclusion that several-GPa equilibration pressures are required to reproduce the oxidized nature of Group 2 angrites is robust across existing models because they consistently predict an increase in $Fe^{3+}/\Sigma Fe$ with pressure above ~5 GPa.

$Fe^{3+}/\Sigma Fe$ ratios of the primitive Group 1 angrite magma (Table A3) (F. L. H. Tissot et al. 2022) at ΔIW–1.4 ± 0.5 (E. S. Steenstra et al. 2017) were calculated as a function of the assumed CMEP with 1 GPa step. Temperature conditions of the CMEP were assumed to be intermediate values between the solidus (C. Herzberg et al. 2000) and liquidus (C. Herzberg & J. Zhang 1996; D. Andrault et al. 2018 and references therein) temperatures of peridotite, similar to the canonical core-formation model (D. C. Rubie et al. 2015) (Figure A1).

2.3. Fractional Crystallization Model

We followed the crystallization sequence of Group 1 angrite magmas (i.e., NWA 1670 and LEW 87051) to reproduce the composition of Group 2 angrites (D'Orbigny, Sahara 99555, and NWA 1296). In this sequence, olivine crystallized first, followed by olivine + plagioclase at melt fractions <0.82, and olivine + plagioclase + clinopyroxene at melt fractions <0.72, similar to the sequence used in F. L. H. Tissot et al. (2022). The mass concentrations of oxides (MgO, FeO, and Fe_2O_3) in the residual melt at step n were calculated by the following equation.

$$C_i^{Melt}{}_n = \frac{F_i^{Melt}{}_{n-1}C_i^{Melt}{}_{n-1} - D_i^{Bulk}{}_{n-1}C_i^{Melt}{}_{n-1}(F_i^{Melt}{}_{n-1} - F_i^{Melt}{}_n)}{F_i^{Melt}{}_n}. \quad (4)$$

Here, $C_i^{Melt}{}_n$, $F_i^{Melt}{}_n$, and $D_i^{Bulk}{}_n$ are the mass concentration, mass fraction, and bulk solid–liquid partition coefficient of oxide i at the step n, respectively. $D_i^{Bulk}{}_n$ was estimated from the modal abundances of minerals and their respective compositions or solid–liquid partition coefficients as

$$D_i^{Bulk}{}_{n-1} = \frac{F^{Ol}C_i^{Ol}{}_{n-1} + F^{Pl}C_i^{Pl}{}_{n-1} + F^{Cpx}C_i^{Cpx}{}_{n-1}}{C_i^{Melt}{}_{n-1}}. \quad (5)$$

In this calculation, olivine composition was estimated using the Fe^{2+}–Mg distribution coefficient (K_D) of 0.33 (F. L. H. Tissot et al. 2022). The compositions of plagioclase and clinopyroxene were assumed to remain constant, adopting pure anorthite and a representative core composition of clinopyroxene in Group 1 angrites (11.68 wt% FeO and 8.99 wt% MgO; D'Orbigny and Asuka 881371) estimated by F. L. H. Tissot et al. (2022) and references therein. For Fe_2O_3 in the residual melts, we assumed that all Fe_2O_3 remains entirely in the melt prior to clinopyroxene saturation. After clinopyroxene saturation, Fe_2O_3 in the melt was calculated using the partition coefficient of 0.78 for clinopyroxene (F. A. Davis & E. Cottrell 2021).

Several aspects of this parameterization are experimentally motivated. First, olivine is nearly free of Fe^{3+}, even under the relatively oxidized conditions of Earth's upper mantle (e.g., D. Canil & H. S. C. O'Neill 1996; A. B. Woodland et al. 2006), making Fe^{3+} incorporation into olivine in more reduced angritic systems negligible. Second, the absence of any Fe^{3+}-bearing phase (e.g., spinel) during the early olivine + plagioclase crystallization stages supports the assumption that Fe^{3+} remains in the melt until clinopyroxene saturation. Third, the Fe^{3+} partition coefficient for clinopyroxene (0.78) has been shown to remain constant over a wide fO_2 range (ΔFMQ −3 to +3; F. A. Davis & E. Cottrell 2021), supporting its applicability to angritic redox conditions. Despite these simplifications, our model successfully reproduces the major-element composition (Mg#) of Group 2 angrites, supporting the internal consistency of the framework. Melt compositions were calculated at 2 wt% melt-fraction increments using a stepwise mass-balance fractional crystallization approach (Equations (4) and (5)), in which extracted solids are removed from the system at each step and the residual melt composition

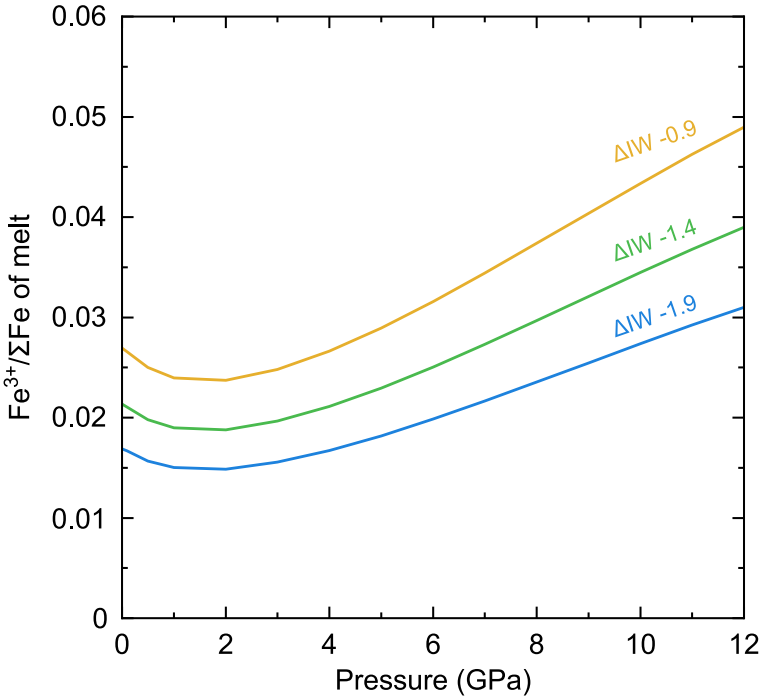

Figure 2. The effect of pressure on $Fe^{3+}/\Sigma Fe$ ratio of Group 1 angrite magma. Each color indicates fO_2 at the core–mantle equilibration based on the estimation by E. S. Steenstra et al. (2017).

is recalculated. Parameters used in the fractional crystallization model are summarized in Table A4.

2.4. fO_2 Estimation for Group 1 and 2 Angrites

Based on the thermodynamic modeling of phase diagram for Group 1 angrites (F. L. H. Tissot et al. 2022), NWA 1670 and LEW 87051 have the olivine-orthopyroxene multiple-saturation point near their liquidus at 2–3 GPa, suggesting that these angrite magmas could have been in equilibrium with a lherzolite-like mantle mineral assemblage prior to eruption. This is consistent with Group 1 angrites representing primary magmas of the APB mantle. Thus, we assumed that the averaged composition of NWA 1670 and LEW 87051 represents the APB magma ocean (Table A3). The fO_2 of the averaged Group 1 angrite magmas was estimated under their melting *P–T* conditions, i.e., at the olivine-orthopyroxene multiple saturation near the liquidus (i.e., 2 GPa and 1673–1873 K) (F. L. H. Tissot et al. 2022), using C. Sun & L. Yao's (2024) thermodynamic model. For the fO_2 estimation of Group 2 angrites, we used $Fe^{3+}/\Sigma Fe$ ratios of residual magmas produced by fractional crystallization of Group 1 angrites at melt fractions $= 0.5 \pm 0.1$, where the Mg# of the residual magma is consistent with that of Group 2 angrites. The fO_2 was calculated at 0.7 GPa and 1473 K, which is within the restricted *P–T* conditions for the formation of Group 2 angrite magmas, i.e., the olivine-clinopyroxene-plagioclase multiple saturation near the liquidus (i.e., 0.6–0.9 GPa and 1500 ± 30 K) (F. L. H. Tissot et al. 2022).

3. Results

3.1. $Fe^{3+}/\Sigma Fe$ Ratio of Group 1 Angrite Magma Under Metal-saturated Conditions

The results show that $Fe^{3+}/\Sigma Fe$ ratios of the primitive Group 1 angrite magma exhibit a weak pressure dependence below 4 GPa, with a subtle minimum around 2 GPa, followed by a gradual increase with pressure (Figure 2). Over the pressure range of 1 bar to 12 GPa, $Fe^{3+}/\Sigma Fe$ ratios range from 0.015–0.031, 0.019–0.039, and 0.024–0.049 at ΔIW values of –1.9, –1.4, and –0.9, respectively. The reversal in the pressure dependence of the $Fe^{3+}/\Sigma Fe$ ratio around 2–4 GPa reflects competing pressure effects on iron redox equilibria. At low pressures, compression favors the IW buffer reaction more than the reaction (2) ($FeO + 1/4O_2 = FeO_{1.5}$) because the ΔV of the IW buffer reaction is smaller than that of the reaction (2), which produces a net decrease in $Fe^{3+}/\Sigma Fe$ with pressure. Above ~4 GPa, the ΔV of the reaction (2) becomes smaller than that of the IW buffer, so that pressure increasingly stabilizes Fe^{3+} relative to Fe^{2+}, yielding the observed positive pressure dependence at higher pressures.

It is noted that the solidus and liquidus temperatures of angrites may be lower than those of KLB-1 peridotite used in our study because angrites contain higher FeO, which has a negative effect on both solidus and liquidus temperatures, as observed in melting experiments on the Martian mantle composition (M. S. Duncan et al. 2018). Lower-temperature conditions yield lower $Fe^{3+}/\Sigma Fe$ ratios in magmas in our calculation; therefore, higher pressures are necessary to increase $Fe^{3+}/\Sigma Fe$ ratios in magmas. We also tested the bulk silicate angrite composition, which was estimated by considering nebular fractionation (F. L. H. Tissot et al. 2022), and found that the difference in the $Fe^{3+}/\Sigma Fe$ ratio relative to the averaged Group 1 angrite composition is negligible (<0.005) (Figure A2).

In summary, the sensitivity of the inferred CMEPs to the major input parameters is as follows. The initial magma-ocean fO_2 exerts the strongest control: varying the starting redox state from $\Delta IW-0.9$ to $\Delta IW-1.9$ shifts the required CMEP from ~4 GPa to ~10 GPa (Figure 5(a); Supplementary Figures A3–A5). Temperature has a secondary effect, with

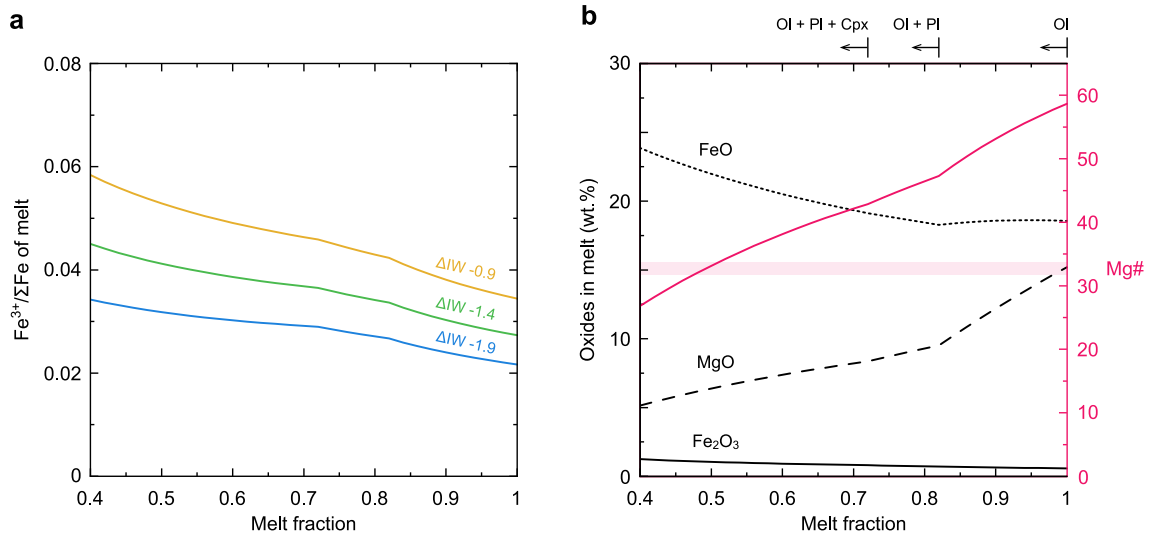

Figure 3. (a) The changes in $Fe^{3+}/\Sigma Fe$ ratio of residual magma during the crystallization of Group 1 angrite magma that is set by the core–mantle equilibration at 7 GPa and (b) chemical composition of the residual magma during crystallization. The pink line indicates the change in Mg# of the residual magma (Mg# = molar Mg/(Fe + Mg)×100). The pink shaded region is the Mg# range of Group 2 angrites.

lower solidus-liquidus temperatures than those assumed here requiring modestly higher equilibration pressures. The starting melt composition has a minor influence: the $Fe^{3+}/\Sigma Fe$ difference between the averaged Group 1 angrite and the bulk silicate angrite composition is <0.005 (Figure A2). Across all plausible parameter combinations, the requirement of several-GPa equilibration pressures to reproduce the oxidized character of Group 2 angrites remains robust, although the exact pressure values are model- and parameter-dependent.

3.2. Fractional Crystallization Effect on the $Fe^{3+}/\Sigma Fe$ Ratio of Residual Magmas

After the core–mantle separation in APB, we calculated the change in the $Fe^{3+}/\Sigma Fe$ ratio of residual magmas during fractional crystallization. We followed the crystallization sequence of F. L. H. Tissot et al. (2022) to reproduce Group 2 angrites (D'Orbigny, Sahara 99555, and NWA 1296) from Group 1 angrites (averaged composition of NWA 1670 and LEW 87051). When the initial $Fe^{3+}/\Sigma Fe$ ratio of Group 1 angrite magmas is set by core–mantle equilibration at 7 GPa and ΔIW–1.4 ± 0.5, the $Fe^{3+}/\Sigma Fe$ ratio of the residual magmas increases from 0.022–0.034 to 0.032–0.053 at melt fraction of 0.5, reproducing the Mg# of Group 2 angrites (Figure 3). The results show that fractional crystallization increases the $Fe^{3+}/\Sigma Fe$ ratio of residual magmas by no more than a factor of two. In our calculations, we assumed that olivine incorporates only Fe^{2+} and that all Fe^{3+} remains in the residual magma. Consequently, olivine crystallization increases the $Fe^{3+}/\Sigma Fe$ ratio of residual magmas. In contrast, subsequent crystallization of plagioclase, which incorporates neither Fe^{2+} nor Fe^{3+}, offsets the enrichment driven by olivine crystallization. Moreover, clinopyroxene incorporates not only Fe^{2+} but also Fe^{3+} (F. A. Davis & E. Cottrell 2021). Therefore, subsequent crystallization of plagioclase and clinopyroxene suppresses the positive effect of olivine crystallization on the $Fe^{3+}/\Sigma Fe$ ratio of the residual magma.

4. Discussion

4.1. Comparison with fO_2 of Group 2 Angrites

Based on the estimated $Fe^{3+}/\Sigma Fe$ ratio of residual magmas, we calculated the fO_2 of Group 2 angrite magmas at 0.7 GPa, which is the middle of estimated formation pressures (0.6–0.9 GPa) (F. L. H. Tissot et al. 2022), and compared them with the fO_2 of Group 2 angrites constrained by the recently developed olivine-spinel-$a^{liq}_{SiO_2}$ oxybarometer ($a^{liq}_{SiO_2}$: SiO_2 activity in the liquid), which can directly apply to angrite lithology (D'Orbigny, Sahara 99555, and NWA 12004; ΔIW +0–0.25; A. S. Bell et al. 2023a).

To reproduce the estimated fO_2 of Group 2 angrites, our calculation results show that CMEPs of 4 ± 1 GPa, 7 ± 1 GPa, and 10 ± 1 GPa are required for redox conditions of ΔIW–0.9, –1.4, and –1.9, respectively (Figure 4; see also Supplementary Figures A3–A5). The results also indicate that Group 2 angrite magmas would retain reducing conditions below the IW buffer for the assumed fO_2 conditions at core–mantle equilibration in our calculations if the core–mantle equilibration occurred at low pressure (<4 GPa). For example, the fO_2 of Group 2 angrite magmas is estimated to be around ΔIW–1 when the core–mantle equilibration occurred at 4 GPa and ΔIW–1.9 (Figure 4). This result is qualitatively consistent with the redox conditions of the lunar mantle (ΔIW–1 ± 0.9 for lunar basalts; H. Zhang et al. 2024b, and ΔIW–1.9 ± 0.2 for core–mantle equilibration; N. Rai & W. van Westrenen 2014), although the Moon's redox evolution may be more complex and may also involve ilmenite cumulate overturn and late volatile addition (e.g., L. T. Elkins-Tanton & T. L. Grove 2011). In addition, Vesta's shallow core–mantle boundary (CMB) (~0.1 GPa) and the estimated fO_2 of core–mantle equilibration (ΔIW–2.2) (E. S. Steenstra et al. 2016) also imply a similarly reduced mantle, further supporting the robustness of our magma-oxidation model. Thus, if internal disproportionation was the dominant oxidizing mechanism, our results indicate that a deep magma ocean for APB (i.e., >4 GPa) is required to account for the relatively oxidized nature of Group 2 angrites (ΔIW > 0) from a starting redox state below ΔIW–1.

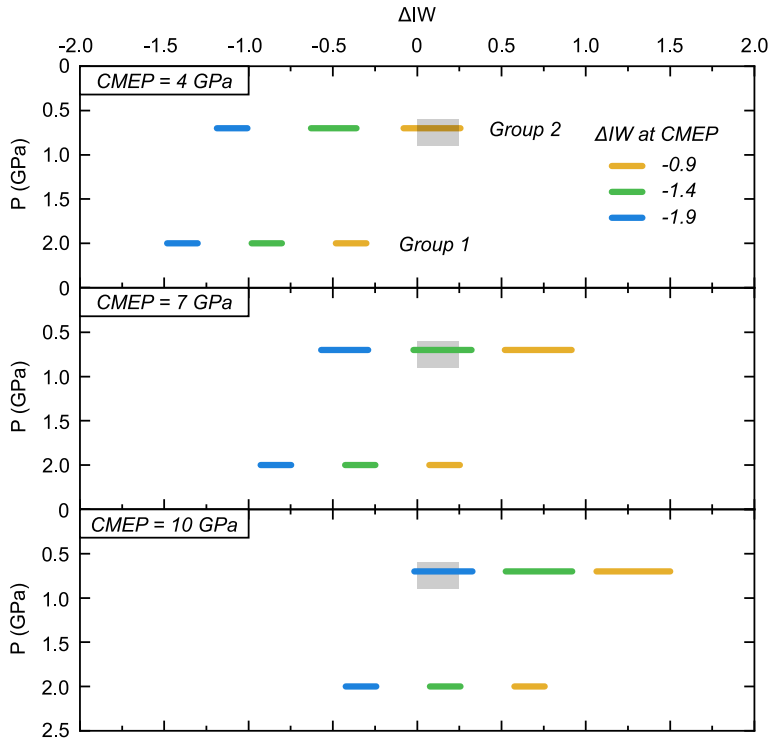

Figure 4. Estimated fO_2 of Group 1 and 2 angrites at their melting P–T conditions for CMEP of 4 GPa, 7 GPa, and 10 GPa. The shaded box region indicates the fO_2 and melting P of Group 2 angrites constrained by the oxybarometer developed in angrite lithology (A. S. Bell et al. 2023a) and the multiple-saturation point (F. L. H. Tissot et al. 2022). Each color indicates the magma-ocean fO_2 during the core formation. CMEP conditions of 4 GPa, 7 GPa, and 10 GPa are necessary to explain the fO_2 of Group 2 angrites at the magma-ocean fO_2 of ΔIW–1.9 to –0.9.

4.2. Inferred fO_2 of Group 1 Angrites

In contrast to Group 2 angrites, the fO_2 of Group 1 angrites (e.g., NWA 1670 and LEW 87051) remains poorly constrained. However, our results suggest that their magmas may have recorded relatively reducing conditions, around ΔIW–0.5 (Figure 4), which is consistent with the presence of Fe-Ni metal in some Group 1 angrites (e.g., NWA 1670 and LEW 87051; K. Keil 2012, and references therein). Another Group 1 angrite, NWA 12774, has been reported to record slightly lower fO_2 values (ΔIW = –0.9 ± 0.2; A. S. Bell et al. 2023b) than those inferred in this study. Although the origin of this difference remains unclear, the relatively high Cr_2O_3 contents of NWA 12774 (Y. He et al. 2024) and their potential role in the reduction of Fe^{3+} in magma during cooling (M. M. Hirschmann 2022) may provide a possible explanation for its lower inferred fO_2. Additional constraints on the redox conditions of other Group 1 angrites, particularly NWA 1670 and LEW 87051, are required to better assess the range and variability of fO_2 within this group.

4.3. Potential Size of APB Permitted by the Magma Self-oxidation Model

To estimate the range of APB sizes compatible with our redox model, we converted CMB pressures into planetary radii using simple interior profiles. Assuming that the CMEP is equivalent to the CMB pressure after APB crystallization, we estimated the size of APB as a function of the CMB pressure. The pressure at a given depth z inside the body is estimated by the following equation:

$$P(z) = \int_0^z \rho(z) g(z) dz. \quad (6)$$

Here, $P(z)$, $\rho(z)$, and $g(z)$ are the pressure, density, and gravitational acceleration at a given depth z, respectively. $g(z)$ is estimated as follows.

$$g(z) = -\frac{GM(z)}{(R-z)^2} \quad (7)$$

G, $M(z)$, and R are the gravitational constant (6.674×10^{-11} Nm^2/kg^2), the mass below the depth z, and body radius, respectively. For the calculation, we followed F. L. H. Tissot et al. (2022) and assumed the mean mantle density of 3.3–3.5 g cm^{-3}, corresponding to Fo_{100}–Fo_{80} olivine compositions, and the mean core density of 7.5–8.1 g cm^{-3} without considering the effects of temperature, pressure, or the physical state (solid or liquid) of the core on density as a first approximation (Table A5). The representative mean core densities were adopted from F. L. H. Tissot et al. (2022), who estimated these values for the $Fe_{80}Ni_{20}$–$Fe_{70}Ni_{20}S_5C_5$ core compositions inferred by E. S. Steenstra et al. (2017). The assumption of constant mantle and core density is likely robust because the pressure range considered here is below the olivine phase transition pressure (i.e., 14 GPa) and density increase by compression at higher pressures may be compensated or minimized by thermal expansion at higher temperatures in the depth. This inference is consistent with the nearly constant density profiles for the Moon (~3.4 g cm^{-3}, R. C. Weber et al. 2011) and Mars (~3.5–3.6 g cm^{-3} at depth below the olivine phase transition, A. Khan et al. 2023; H. Samuel et al. 2023). Assuming core-mass fractions of 0.1–0.3, the CMB pressure was calculated as a function of the body radius (Figure 5; see also Supplementary Figure A6). It is

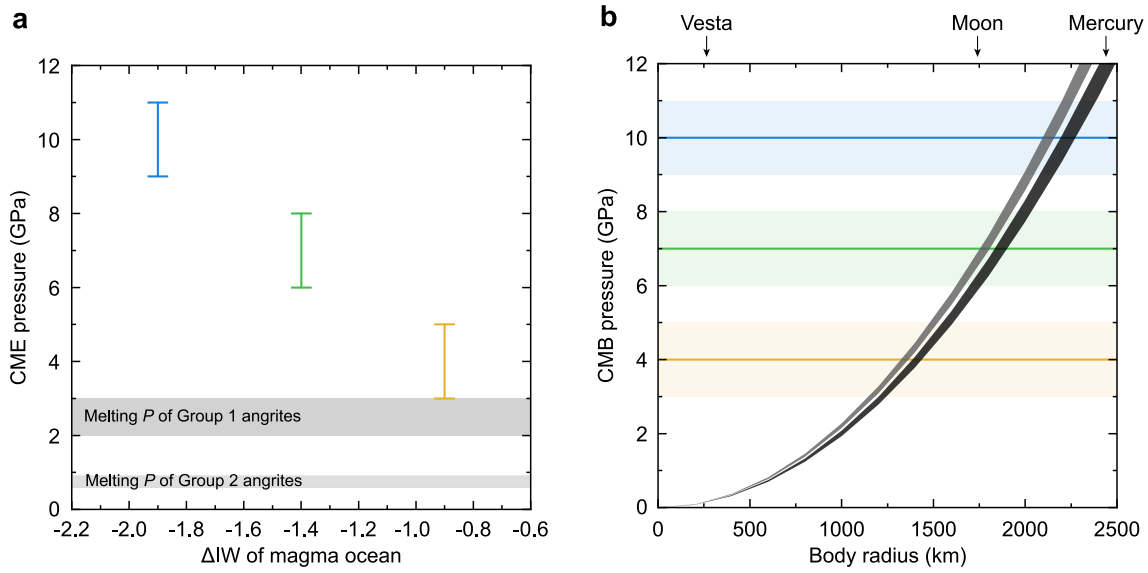

Figure 5. (a) Estimated CMEP as a function of the magma-ocean fO_2 and (b) CMB pressure as a function of body radius. Gray and black shaded curves indicate the results using 3.5 g cm^{-3} and 3.3 g cm^{-3} for mantle density with 8.1 g cm^{-3} of the core density and 0.1–0.3 core-mass fraction, respectively.

also noted that a possible change in the core density by the presence of light elements does not significantly affect the relationship between the CMB pressure and body radius (Figure A6). For each choice of initial redox state and pressure of the core–mantle equilibration in the APB magma ocean, we then followed fractional crystallization and tracked the evolution of $Fe^{3+}/\Sigma Fe$ until the calculated fO_2 matched that of evolved (Group 2) angrites. This approach yields a family of solutions rather than a single best-fit size: for moderately reduced starting conditions, CMB pressures of order 4–7 GPa are required to reproduce the observed fO_2, implying radii substantially greater than Vesta (Figure 5(b)) and overlapping the range inferred from independent geobarometry of angrites.

These redox-based size estimates are independently supported by CaTs-liquid clinopyroxene geobarometry, which yields crystallization pressures of ∼15–18 kbar and a minimum APB radius of ∼1000 km (A. S. Bell et al. 2026), and by multiple saturation pressure constraints indicating an embryo-scale APB (F. L. H. Tissot et al. 2022). The convergence of three independent approaches—redox modeling, clinopyroxene barometry, and phase equilibria—strengthens the case for an embryo-scale APB. A large APB, as inferred from magma self-oxidation model, would also be qualitatively consistent with the elevated HSE abundances of the APB mantle relative to Vesta (C. W. Dale et al. 2012) because larger bodies more efficiently capture late-accreting material (W. F. Bottke et al. 2010; M.-H. Zhu et al. 2021). However, HSE abundances alone do not uniquely constrain parent-body size because the efficiency of HSE retention depends on additional factors such as impact velocity, retention efficiency, and the timing and duration of late accretion. Our interpretation of a large APB is further supported by the presence of solar-like noble gases in angrite glasses (H. Busemann et al. 2006), which may reflect gravitational capture of nebular gases, a process only feasible for bodies with substantial mass, larger than the Moon (R. O. Pepin & D. Porcelli 2002). Moreover, dunitic angrite NWA 8535, likely originating from the APB mantle, records the youngest Pb–Pb age of 4514 ± 30 Myr (B. G. Rider-Stokes et al. 2024b), indicating prolonged magmatism on APB after its formation (∼50 Myr). Consistently, cosmic-ray exposure ages of volcanic and plutonic angrites are uniformly distributed in a comparable timescale (∼56 Myr) (D. Nakashima et al. 2018), suggesting that APB was probably large enough to sustain magmatic activity and avoid catastrophic disruption for at least ∼50 Myr after its formation.

The APB is currently unidentified among known asteroids. Recent UV–vis-NIR spectroscopic surveys of asteroids have found no large body with angrite-like surface properties; the closest spectral match was a small (∼50 km) asteroid (B. G. Rider-Stokes et al. 2025). The absence of a large surviving body with angrite-like spectra is consistent with the broader "missing mantle" problem, in which olivine-rich differentiated material is underrepresented among observed asteroids, despite predictions from planetary differentiation models. This suggests that the APB was either incorporated into the growing terrestrial planets during late-stage accretion or disrupted into fragments too small to be spectrally identified. The magma self-oxidation mechanism proposed here should in principle be applicable to any embryo-scale body that formed a deep magma ocean with CMEPs exceeding several gigapascals, although the specific redox evolution would depend on each body's bulk composition, volatile budget, and accretion history. To further constrain a possible disruption event on the APB, searching for olivine-rich asteroids and performing additional spectroscopic comparisons with angrites may be important.

4.4. Limitations and Alternative Redox Scenarios

Our inferences are subject to several important limitations that should be borne in mind when interpreting the size of the APB. First, most existing fO_2 estimates for angrites are derived from evolved, fractionated magmas and late-stage assemblages. These melts are susceptible to auto-oxidation, degassing, and local heterogeneities, and may not uniquely record the redox state of the deep mantle. Primitive angrites, including those with metal-rich mineralogies, suggest that at least part of the APB interior remained substantially reduced,

consistent with a redox stratigraphy in which deep reservoirs are more reduced than the shallow magmatic system sampled by evolved lavas. Our modeling should therefore be viewed as quantifying the conditions required to generate the shallow angrite magmas and not as a direct inversion of the bulk mantle fO_2.

Second, internal magma self-oxidation is not the only process capable of modifying fO_2. Inherited redox conditions from precursor materials, interaction with volatile-bearing phases, and open-system degassing could all contribute to the redox evolution of angrite magmas. In particular, if the primitive APB mantle was H_2O rich (as suggested by the D/H ratio of NWA 4801; B. G. Rider-Stokes et al. 2024a), then H_2 loss and outgassing during decompression and cooling could have contributed to mantle oxidation independently of high-pressure disproportionation (see Z. C. Sharp et al. 2013). Similarly, even in the absence of any postcore formation process, the oxidation state of the primitive APB mantle might simply reflect the inherited redox properties of its accretionary feedstock. We cannot currently distinguish among these end-member scenarios with existing data. We have focused here on the end-member case in which internal disproportionation is the dominant oxidizing mechanism, and our size estimates should therefore be regarded as scenario-dependent lower bounds rather than unique solutions.

Despite these caveats, the redox-based constraints derived here are complementary to independent geobarometric estimates and together point toward an APB that lies firmly in the embryo regime. Future work combining high-precision fO_2 determinations for both primitive and evolved angrites, improved $Fe^{3+}/\Sigma Fe$ measurements at high pressures, and metal-silicate partitioning of moderately siderophile elements combined with dynamical models of early inner solar system accretion will be essential to refine these bounds and to establish how common such embryo-scale bodies were during the earliest stages of terrestrial planet formation.

5. Concluding Remarks

In summary, the APB likely experienced a magma-ocean phase and early core–mantle differentiation under moderately reduced conditions, followed by internal magma self-oxidation and fractional crystallization that produced the evolved angrite magmas we observe today. By combining experimentally and theoretically constrained $Fe^{3+}/\Sigma Fe$-pressure relations with angrite geochemistry, we show that reproducing the redox state of evolved angrites through internal processes alone requires core–mantle equilibration at several gigapascals, implying an APB with minimum radii of ∼1250–2500 km, comparable to or exceeding the size of the Moon, and overlapping independent geobarometric estimates. These size estimates are scenario-dependent lower bounds, contingent on the assumption that FeO disproportionation was the dominant oxidation mechanism; alternative scenarios involving inherited feedstock redox or volatile-driven oxidation could modify the required pressures. This scenario suggests that some rocky bodies in the inner solar system rapidly accreted to embryo scale within the first few million years and then either merged into the growing terrestrial planets or were disrupted into smaller fragments. Targeted spectroscopic searches for angrite-like surfaces, improved experimental constraints on $Fe^{3+}/\Sigma Fe$ at high pressure, and more precise fO_2 estimates for both primitive and evolved angrites will further test this picture and help to better constrain the population and evolution of early planetary embryos.

Acknowledgments

This study was supported by the Japan Society of the Promotion of Science (JSPS) KAKENHI to H.K. (grant Nos. 24K00737 and 25K22048) and startup funds by Yale University to D.S.G.

Author Contributions

H.K. conceived the idea, collected data, and conducted calculations. H.K. and D.S.G. wrote the manuscript with help of K.T. All authors discussed the results and commented on the manuscript.

Appendix

A.1. Mantle f_{O_2} of Rocky Bodies

The fO_2 of magma ocean and CMEPs for Vesta (E. S. Steenstra et al. 2016), APB (E. S. Steenstra et al. 2017), Moon (N. Rai & W. van Westrenen 2014), Mars (K. Righter & N. L. Chabot 2011; M. M. Hirschmann 2022), and Earth (K. Righter 2011; M. M. Hirschmann 2022) have been estimated by previous experimental studies based on the FeO content of the mantle or the metal-silicate partitioning of siderophile elements, such as Ni and Co. According to these studies, CMEPs for Vesta and Moon were assumed to be 0.1 GPa and 5 GPa, respectively. The CMEP of the Earth may have been higher than the estimate of K. Righter (2011) (i.e., 30 ± 3 GPa) (J. Wade & B. J. Wood 2005; R. A. Fischer et al. 2015), but the positive relationship between the size of body and mantle fO_2 remains unchanged. The fO_2 of the mantles of Vesta (A. J. G. Jurewicz et al. 1993; M. Wadhwa 2008), Moon (M. Wadhwa 2008; H. Zhang et al. 2024b), Mars (M. Wadhwa 2008; R. W. Nicklas et al. 2021), and Earth (D. J. Frost et al. 2008 and references therein) have been estimated in previous studies using meteorites and solid–liquid partitioning of redox-sensitive elements, such as Eu and V.

A.2. Supplementary Material

Magma ocean fO2, CMEPs, and mantle fO2 values of rocky bodies in the solar system estimated in previous studies are summarized in Tables A1 and A2. The averaged Group 1 angrite composition used in our calculations and the estimated bulk silicate angrite composition are shown in Table A3. The parameters used in our fractional crystallization model and for estimating the size of the APB are summarized in Tables A4 and A5.

Figures A1 and A2 show the temperature conditions used to estimate the Fe3+/ΣFe ratio of the APB magma ocean and the estimated Fe3+/ΣFe ratios under given pressure conditions for the averaged Group 1 angrite and bulk silicate angrite compositions. Figures A3, A4, and A5 show the estimated fO2 of Group 1 and 2 angrites for CMEP conditions of 3–5 GPa, 6–8 GPa, and 9–11 GPa, respectively. Figure A6 shows the effect of core composition on the estimated relationship between CMB pressure and the radius of the APB.

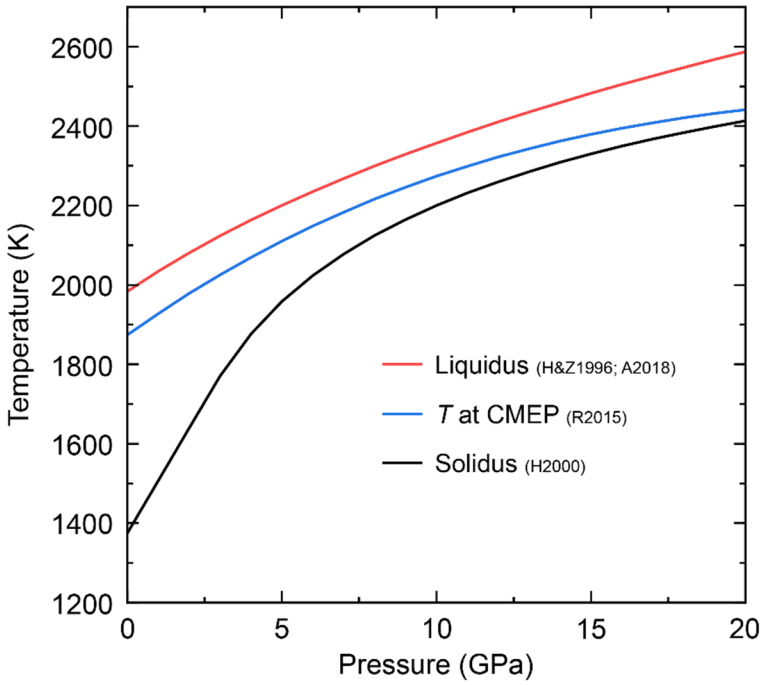

Figure A1. Temperature conditions used for calculation of fO_2. Solidus temperature shown as H2000 was taken from C. Herzberg et al. (2000). Liquidus temperature shown as H&Z1996; A2018 was taken from C. Herzberg & J. Zhang (1996) and D. Andrault et al. (2018). Temperature at the CMEP shown as R2015 was taken from D. C. Rubie et al. (2015).

Table A1
Estimated Magma-ocean fO_2 and CMEP of Rocky Bodies

	ΔIW[a]	Error	References	CMEP (GPa)	Error	References
Vesta	−2.2	0.2	E. S. Steenstra et al. (2016)	∼0.1[b]	…	E. S. Steenstra et al. (2016)
Moon	−1.9	0.2	N. Rai & W. van Westrenen (2014)	∼5[b]	…	N. Rai & W. van Westrenen (2014)
Mars	−1.4	0.2	M. M. Hirschmann (2022)	14	3	K. Righter & N. L. Chabot (2011)
Earth	−2	0.6	M. M. Hirschmann (2022)	30	3	K. Righter (2011)
APB	−1.4	0.5	E. S. Steenstra et al. (2017)	…	…	…
NC IMPBs	−2.2[c]	0.5	D. S. Grewal et al. (2024)	<0.1	…	D. S. Grewal et al. (2022a)
CC IMPBs	−1.6[d]	0.4	D. S. Grewal et al. (2024)	<0.1	…	D. S. Grewal et al. (2022a)

Notes.
[a] fO_2 relative to the IW buffer in log units.
[b] CMEP is assumed to be identical to the CMB.
[c] Averaged values of NC IMPBs.
[d] Averaged values of CC IMPBs.

Table A2
Estimated Mantle fO_2 of Rocky Bodies

	ΔIW	Error	References
Vesta	−1.0	…	A. J. G. Jurewicz et al. (1993), M. Wadhwa (2008)
Moon	−1.0	0.9	H. Zhang et al. (2024b)
Mars	1.4	1.8	R. W. Nicklas et al. (2021)
Earth	3.75	1.75	D. J. Frost et al. (2008)

Table A3
Chemical Compositions of the Averaged Primitive Group 1 Angrites (i.e., LEW 87051 and NWA 1670) and the Estimated Bulk Silicate Angrite (wt%) (F. L. H. Tissot et al. 2022 and References Therein)

Oxide	Group 1 Angrite	Bulk Silicate Angrite
SiO_2	41.16	38.29
TiO_2	0.67	0.20
Al_2O_3	11.07	3.80
Cr_2O_3	0.14–0.45[a]	0.30
MgO	15.20	33.13
FeO	19.09	20.69
CaO	11.89	3.59

Note.
[a] Upper estimate is the value of NWA 12774 taken from Y. He et al. (2024).

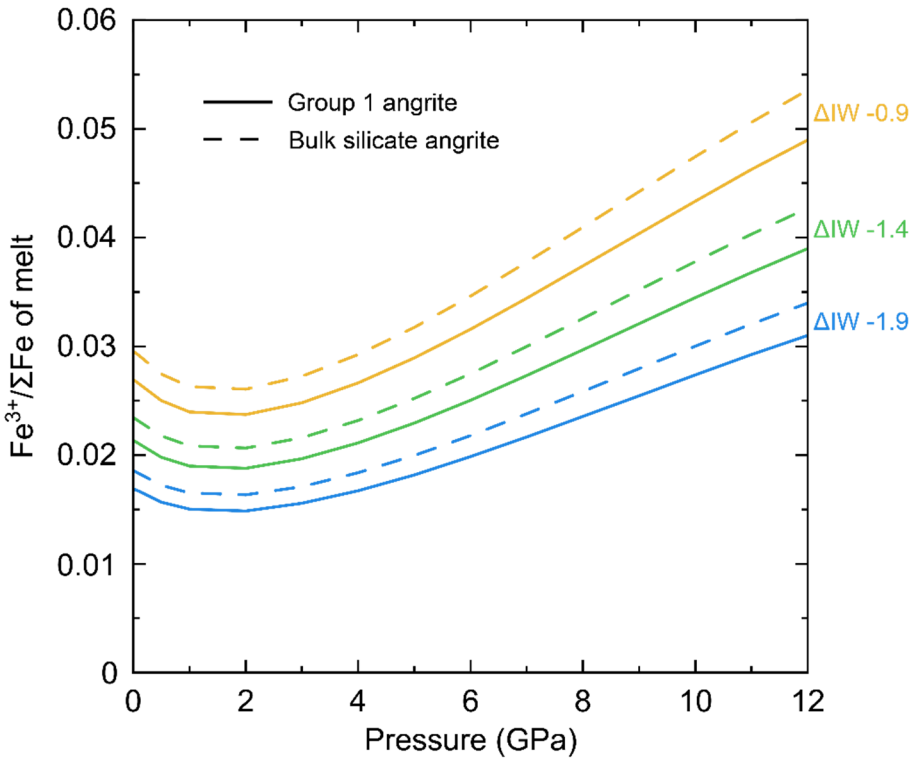

Figure A2. The effect of pressure on $Fe^{3+}/\Sigma Fe$ ratios of Group 1 angrite and estimated bulk silicate angrite magmas. Each color indicates fO_2 at the core–mantle equilibration based on the estimation by E. S. Steenstra et al. (2017).

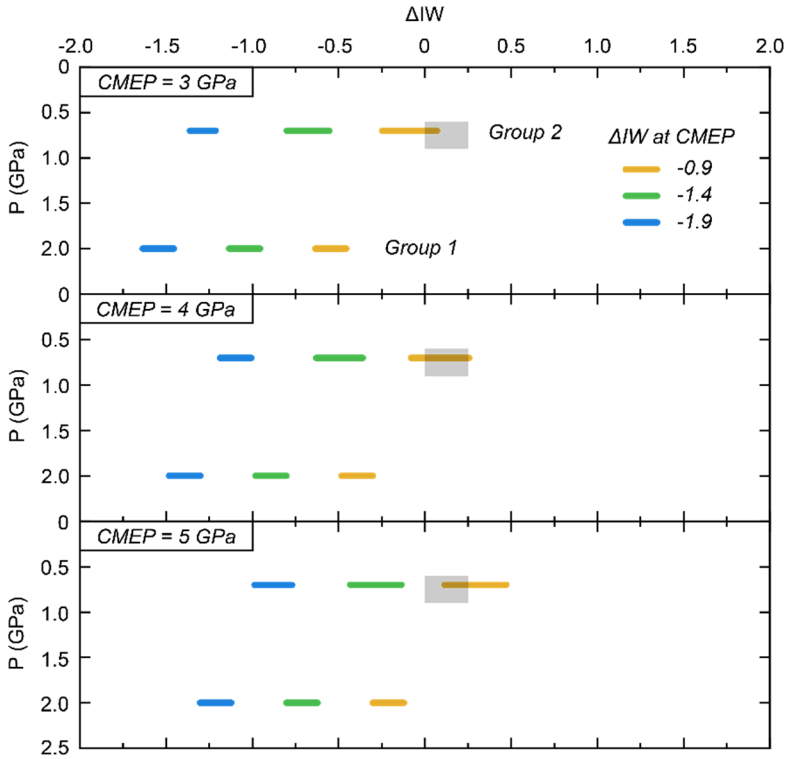

Figure A3. Estimated fO_2 of Group 1 and 2 angrites at their melting P–T conditions for CMEP of 3–5 GPa. These conditions reproduce the fO_2 of Group 2 angrites (A. S. Bell et al. 2023a) when the magma-ocean fO_2 was ΔIW–0.9.

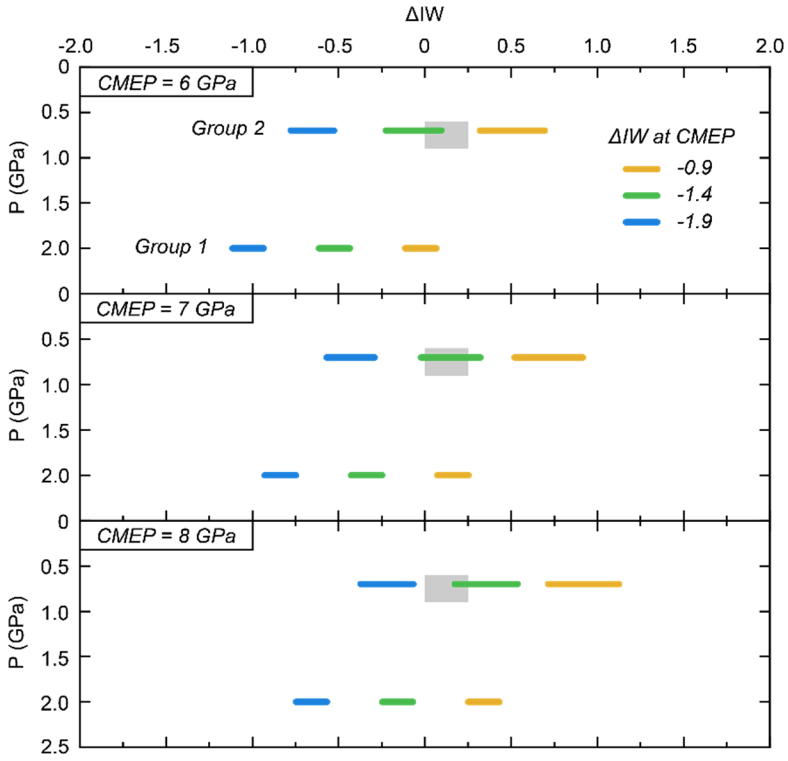

Figure A4. Estimated fO_2 of Group 1 and 2 angrites at their melting P–T conditions for CMEP of 6–8 GPa. These conditions reproduce the fO_2 of Group 2 angrites (A. S. Bell et al. 2023a) when the magma-ocean fO_2 was ΔIW–1.4.

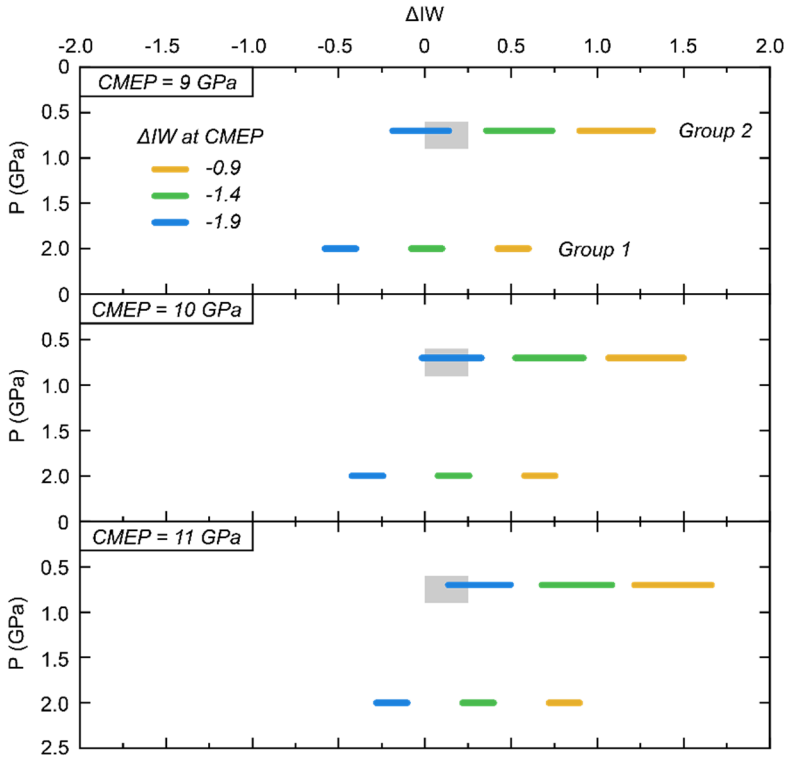

Figure A5. Estimated fO_2 of Group 1 and 2 angrites at their melting P–T conditions for CMEP of 9–11 GPa. These conditions reproduce the fO_2 of Group 2 angrites (A. S. Bell et al. 2023a) when the magma-ocean fO_2 was ΔIW–1.9.

Table A4
Parameters Used for Fractional Crystallization Model

Parameters	Value			References
K_D[a]	0.33			F. L. H. Tissot et al. (2022)
$D^{Cpx}_{Fe_2O_3}$	0.78			F. A. Davis & E. Cottrell (2021)
Mass fraction (%)	$F^{Melt} = 1 \rightarrow 0.82$	$F^{Melt} = 0.82 \rightarrow 0.72$	$F^{Melt} = 0.72 \rightarrow 0.4$	
F^{Ol}	100	48.4	30	F. L. H. Tissot et al. (2022)
F^{Pl}	0	51.6	38	
F^{Cpx}	0	0	32	

Note.
[a] The Fe^{2+}-Mg distribution coefficient between olivine and silicate melt.

Table A5
Parameters Used for Estimating the Size of APB

Parameters	Value
G[a]	6.674×10^{-11} Nm^2/kg^2
ρ_{mantle}[b]	3.3–3.5 g cm^{-3}
ρ_{core}[c]	7.5–8.1 g cm^{-3}

Notes.
[a] The gravitational constant.
[b] Fo_{100}–Fo_{80} olivine composition.
[c] $Fe_{80}Ni_{20}$–$Fe_{70}Ni_{20}C_5S_5$ composition

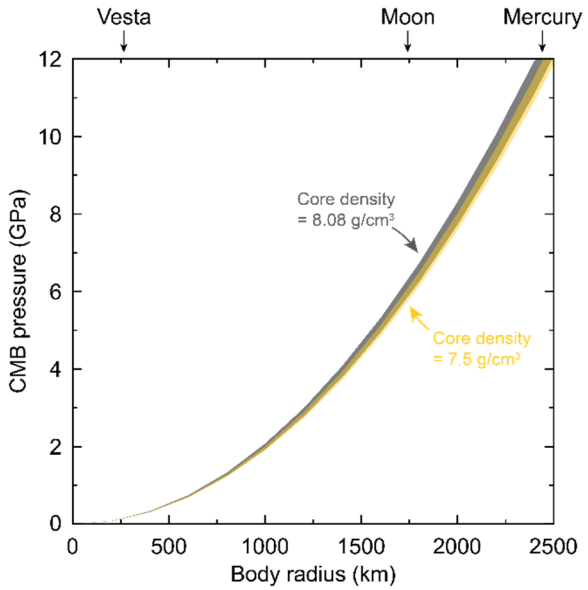

Figure A6. The effect of light elements in the core on the relationship between CMB pressure and body radius. Gray and yellow shaded curves indicate the results using 8.1 g cm^{-3} ($Fe_{80}Ni_{20}$ composition) and 7.5 g cm^{-3} ($Fe_{70}Ni_{20}S_5C_5$ composition) for core density with 3.3 g cm^{-3} for mantle density and 0.1–0.3 core-mass fraction, respectively.

ORCID iDs

Hideharu Kuwahara https://orcid.org/0000-0001-9379-3529
Damanveer S. Grewal https://orcid.org/0000-0002-5653-1543

References

Abernethy, F. A. J., Verchovsky, A. B., Starkey, N. A., et al. 2013, Stable Isotope Analysis of Carbon and Nitrogen in Angrites, M&PS, 48, 1590
Abernethy, F. A. J., Verchovsky, A. B., Franchi, I. A., & Grady, M. M. 2018, Basaltic Volcanism on the Angrite Parent Body: Comparison with Vesta, M&PS, 53, 375
Alexander, C. M. Q. 'D. 2019, Quantitative Models for the Elemental and Isotopic Fractionations in the Chondrites: The Non-carbonaceous Chondrites, GeCoA, 254, 246
Andrault, D., Pesce, G., Manthilake, G., et al. 2018, Deep and Persistent Melt Layer in the Archean Mantle, NatGe, 11, 139
Armstrong, K., Frost, D. J., McCammon, C. A., Rubie, D. C., & Boffa Ballaran, T. 2019, Deep Magma Ocean Formation Set the Oxidation State of Earth's Mantle, Sci, 365, 903
Bell, A. S., Shearer, C., Pinkham, L., & Irving, A. J. 2023a, Appraising the Late-stage Magmatic fO_2 of Diabasic Angrites with a Novel Phase Equilibrium Approach: Implications for New and Existing Models of Angrite Petrogenesis, GeCoA, 348, 140
Bell, A. S., Pinkham, L., Shearer, C., & Irving, A. 2023b, New Cr K-edge XANES and Phase Equilibrium Constraints on Primitive Magmatic Redox Conditions on the Angrite Parent Body and Implications for Core Formation, in Goldschmidt 2023 Conf. (EAG), 15458
Bell, A. S., Waters, L., & Ghiorso, M. 2026, High-pressure Clinopyroxene in Northwest Africa 12774 and New Geobarometric Evidence for a Planetary Embryo-sized Angrite Parent Body, E&PSL, 685, 120029
Binzel, R. P., & Xu, S. 1993, Chips off of Asteroid Vesta: Evidence for the Parent Body of Basaltic Achondrite Meteorites, Sci, 260, 186
Bottke, W. F., Walker, R. J., Day, J. M. D., Nesvorny, D., & Elkins-Tanton, L. 2010, Stochastic Late Accretion to Earth, the Moon, and Mars, Sci, 330, 1527
Busemann, H., Lorenzetti, S., & Eugster, O. 2006, Noble Gases in D'Orbigny, Sahara 99555 and D'Orbigny Glass: Evidence for Early Planetary Processing on the Angrite Parent Body, GeCoA, 70, 5403
Canil, D., & O'Neill, H. S. C. 1996, Distribution of Ferric Iron in Some Upper-mantle Assemblages, JPet, 37, 609
Canup, R. M., & Asphaug, E. 2001, Origin of the Moon in a Giant Impact Near the End of the Earth's Formation, Natur, 412, 708
Cao, Z., Guo, Z., Li, C., et al. 2024, Submicroscopic Magnetite may be Ubiquitous in the Lunar Regolith of the High-Ti Region, SciA, 10, eadn2301
Chambers, J. M., & Wetherill, G. W. 1998, Making the Terrestrial Planets: N-body Integrations of Planetary Embryos in Three Dimensions, Icar, 316, 304
Dale, C. W., Burton, K. W., Greenwood, R. C., et al. 2012, Late Accretion on the Earliest Planetesimals Revealed by the Highly Siderophile Elements, Sci, 336, 72
Davis, F. A., & Cottrell, E. 2021, Partitioning of Fe_2O_3 in Peridotite Partial Melting Experiments Over a Range of Oxygen Fugacities Elucidates Ferric Iron Systematics in Mid-ocean Ridge Basalts and Ferric Iron Content of the Upper Mantle, CoMP, 176, 67
Deng, J., Du, Z. X., Karki, B. B., Ghosh, D. B., & Lee, K. K. M. 2020, A Magma Ocean Origin to Divergent Redox Evolutions of Rocky Planetary Bodies and Early Atmosphere, NatCo, 11, 2007
Duncan, M. S., Schmerr, N. C., Bertka, C. M., & Fei, Y. 2018, Extending the Solidus for a Model Iron-rich Martian Mantle Composition to 25 GPa, GeoRL, 45, 10211
Elkins-Tanton, L. T., & Grove, T. L. 2011, Water (Hydrogen) in the Lunar Mantle: Results from Petrology and Magma Ocean Modeling, E&PSL, 307, 173
Fischer, R. A., Nakajima, Y., Campbell, A. J., et al. 2015, High Pressure Metal–Silicate Partitioning of Ni, Co, V, Cr, Si, and O, GeCoA, 167, 177
Frost, D. J., Mann, U., Asahara, Y., & Rubie, D. C. 2008, The Redox State of the Mantle During and Just After Core Formation, RSPTA, 366, 4315

Fu, R. R., & Elkins-Tanton, L. T. 2014, The Fate of Magmas in Planetesimals and the Retention of Primitive Chondritic Crusts, E&PSL, 390, 128
Greenwood, R. C., Franchi, I. A., Jambon, A., & Buchanan, P. C. 2005, Widespread Magma Oceans on Asteroidal Bodies in the Early Solar System, Natur, 435, 916
Grewal, D. S. 2022, Origin of Nitrogen Isotopic Variations in the Rocky Bodies of the Solar System, ApJ, 937, 123
Grewal, D. S., Xie, N. X., Zhang, B., Izidoro, A., & Asimow, P. D. 2024, Accretion of the Earliest Inner Solar System Planetesimals Beyond the Water Snowline, NatAs, 8, 290
Grewal, D. S., Bhattacharjee, S., Zhang, B., Nie, N. X., & Miyazaki, Y. 2025a, Enrichment of Moderately Volatile Elements in First-generation Planetesimals of the Inner Solar System, SciA, 11, eadq7848
Grewal, D. S., Zhang, Z., Manilal, V., et al. 2025b, Protracted Core Formation and Impact Disruptions Shaped the Earliest Outer Solar System Planetesimals, SciA, 11, eadw1668
Grewal, D. S., Dasgupta, R., & Marty, B. 2021a, A Very Early Origin of Nitrogen in Inner Solar System Protoplanets, NatAs, 5, 356
Grewal, D. S., Seales, J., & Dasgupta, R. 2022a, Internal or External Magma Oceans in the Earliest Protoplanets: Perspectives from Nitrogen and Carbon Fractionation, E&PSL, 598, 117847
Grewal, D. S., & Asimow, P. D. 2023, Origin of the Superchondritic Carbon/Nitrogen Ratio of the Bulk Silicate Earth: An Outlook from Iron Meteorites, GeCoA, 344, 146
Grewal, D. S., Bhattacharjee, S., Mardaru, G.-D., & Asimow, P. D. 2025c, Tracing the Origin of Volatiles on Earth Using Nitrogen Isotope Ratios in Iron Meteorites, GeCoA, 388, 34
Grewal, D. S., Dasgupta, R., Hough, T., & Farnell, A. 2021b, Rates of Protoplanetary Accretion and Differentiation Set Nitrogen Budget of Rocky Planets, NatGe, 14, 369
Grewal, D. S., Sun, T., Aithala, S., et al. 2022b, Limited Nitrogen Isotope Fractionation During Core–Mantle Differentiation in Rocky Protoplanets and Planets, GeCoA, 338, 347
Grewal, D. S., & Mukhopadhyay, S. 2025, Using Carbon Isotopes to Track the Origin of Volatiles on Earth and Mars, GeCoA, 408, 12
Halliday, A. N., & Canup, R. M. 2023, The Accretion of Planet Earth, NRvEE, 4, 19
He, Y., Zhang, A.-C., Peng, Y., Liu, J., & Qin, L. 2024, Mineralogical Anatomy of the Cr-rich Quenched Angrite Northwest Africa 12774: Implication to Mantle Heterogeneity, GeCoA, 365, 186
Herzberg, C., Raterron, P., & Zhang, J. 2000, New Experimental Observations on the Anhydrous Solidus for Peridotite KLB-1, GGG, 1, 1051
Herzberg, C., & Zhang, J. 1996, Melting Experiments on Anhydrous Peridotite KLB-1: Compositions of Magmas in the Upper Mantle and Transition Zone, JGRB, 101, 8271
Hirschmann, M. M. 2012, Magma Ocean Influence on Early Atmosphere Mass and Composition, E&PSL, 341, 48
Hirschmann, M. M. 2022, Magma Oceans, Iron and Chromium Redox, and the Origin of Comparatively Oxidized Planetary Mantles, GeCoA, 328, 221
Jurewicz, A. J. G., Mittlefehldt, D. W., & Jones, J. H. 1993, Experimental Partial Melting of the Allende (CV) and Murchison (CM) Chondrites and the Origin of Asteroidal Basalts, GeCoA, 57, 2123
Keil, K. 2012, Angrites, a Small but Diverse Suite of Ancient, Silica-undersaturated Volcanic–Plutonic Mafic Meteorites, and the History of their Parent Asteroid, ChEG, 72, 191
Khan, A., Huang, D., Durán, C., et al. 2023, Evidence for a Liquid Silicate Layer Atop the Martian Core, Natur, 622, 718
Kleine, T., Mezger, K., Münker, C., Palme, H., & Bischoff, A. 2004, ^{182}Hf-^{182}W Isotope Systematics of Chondrites, Eucrites, and Martian Meteorites: Chronology of Core Formation and Early Mantle Differentiation in Vesta and Mars, GeCoA, 68, 2935
Kleine, T., Hans, U., Irving, A. J., & Bourdon, B. 2012, Chronology of the Angrite Parent Body and Implications for Core Formation in Protoplanets, GeCoA, 84, 186
Kuwahara, H., Nakada, R., Kadoya, S., Yoshino, T., & Irifune, T. 2023, Hadean Mantle Oxidation Inferred from Melting of Peridotite Under Lower-mantle Conditions, NatGe, 16, 461
Li, C., Guo, Z., Li, Y., et al. 2022, Impact-driven Disproportionation Origin of Nanophase Iron Particles in Chang'e-5 Lunar Soil Sample, NatAs, 6, 1156
Markowski, A., Quitté, G., Kleine, T., et al. 2007, Hafnium–Tungsten Chronometry of Angrites and the Earliest Evolution of Planetary Objects, E&PSL, 262, 214
McCoy, T. J., Ketcham, R. A., Wilson, L., et al. 2006, Formation of Vesicles in Asteroidal Basaltic Meteorites, E&PSL, 246, 102
McKay, G., Le, L., Wagstaff, J., & Crozaz, G. 1994, Experimental Partitioning of Rare Earth Elements and Strontium: Constraints on Petrogenesis and Redox Conditions During Crystallization of Antarctic Angrite Lewis Cliff 86010, GeCoA, 58, 2911
McKibbin, S. J., & O'Neill, H. S. C. P. 2018, Petrogenesis of D'Orbigny-like Angrite Meteorites and the Role of Spinel in the Angrite Source, M&PS, 53, 306
Morbidelli, A., Lunine, J. I., O'Brien, D. P., Raymond, S. N., & Walsh, K. J. 2012, Building Terrestrial Planets, AREPS, 40, 251
Nakashima, D., Nagao, K., & Irving, A. J. 2018, Noble Gases in Angrites Northwest Africa 1296, 2999/4931, 4590, and 4801: Evolution History Inferred from Noble Gas Signatures, M&PS, 53, 952
Newcombe, M. E., Nielsen, S. G., Peterson, L. D., et al. 2023, Degassing of Early-formed Planetesimals Restricted Water Delivery to Earth, Natur, 615, 854
Nicklas, R. W., Day, J. M. D., Vaci, Z., et al. 2021, Uniform Oxygen Fugacity of Shergottite Mantle Sources and an Oxidized Martian Lithosphere, E&PSL, 564, 116876
Onyett, I. J., Schiller, M., Makhatadze, G. V., et al. 2023, Silicon Isotope Constraints on Terrestrial Planet Accretion, Natur, 619, 539
Ozawa, K., Hirose, K., & Takahashi, Y. 2022, High-pressure XAFS Measurements of the Coordination Environments of Fe^{2+} and Fe^{3+} in Basaltic Glasses, JGRB, 127, e2021JB023902
Pepin, R. O., & Porcelli, D. 2002, Origin of Noble Gases in the Terrestrial Planets, RvMG, 47, 191
Peterson, L. D., Newcombe, M. E., Alexander, C. M. O. 'D., et al. 2023a, The H_2O Content of the Ureilite Parent Body, GeCoA, 340, 141
Peterson, L. D., Newcombe, M. E., Alexander, C. M. O. 'D., et al. 2023b, The H Content of Aubrites: An Evaluation of Bulk versus In Situ Methods for Quantifying Water in Meteorites, E&PSL, 620, 118341
Rai, N., & van Westrenen, W. 2014, Lunar Core Formation: New Constraints from Metal–Silicate Partitioning of Siderophile Elements, E&PSL, 388, 343
Rider-Stokes, B. G., Stephant, A., Anand, M., et al. 2024a, Evidence Against Water Delivery by Impacts within 10 Million Years of Planetesimal Formation, E&PSL, 642, 118860
Rider-Stokes, B. G., Anand, M., White, L. F., et al. 2024b, The Impact History and Prolonged Magmatism of the Angrite Parent Body, M&PS, 59, 23
Rider-Stokes, B. G., Greenwood, R. C., Anand, M., et al. 2023, Impact Mixing Among Rocky Planetesimals in the Early Solar System from Angrite Oxygen Isotopes, NatAs, 7, 836
Rider-Stokes, B. G., Jackson, S. L., Burbine, T. H., et al. 2025, Remnants of a Lost Planetesimal: Searching for the Angrite Parent Body, Icar, 429, 116429
Righter, K., & Drake, M. J. 1997, A Magma Ocean on Vesta: Core Formation and Petrogenesis of Eucrites and Diogenites, M&PS, 32, 929
Righter, K. 2008, Siderophile Element Depletion in the Angrite Parent Body (APB) Mantle: Due to Core Formation?, LPSC, 39, 1936
Righter, K., & Chabot, N. L. 2011, Moderately and Slightly Siderophile Element Constraints on the Depth and Extent of Melting in Early Mars, M&PS, 46, 157
Righter, K. 2011, Prediction of Metal–Silicate Partition Coefficients for Siderophile Elements: An Update and Assessment of PT Conditions for Metal–Silicate Equilibrium During Accretion of the Earth, E&PSL, 304, 158
Rubie, D. C., Jacobson, S. A., Morbidelli, A., et al. 2015, Accretion and Differentiation of the Terrestrial Planets with Implications for the Compositions of Early-formed Solar System Bodies and Accretion of Water, Icar, 248, 89
Samuel, H., Drilleau, M., Rivoldini, A., et al. 2023, Geophysical Evidence for an Enriched Molten Silicate Layer Above Mars's Core, Natur, 622, 712
Sanborn, M. E., & Wadhwa, M. 2021, Trace Element Geochemistry of Coarse-grained Angrites from Northwest Africa: Implications for their Petrogenesis on the Angrite Parent Body, M&PS, 56, 482
Sarafian, A. R., Nielsen, S. G., Marschall, H. R., et al. 2019, The Water and Fluorine Content of Vesta, GeCoA, 266, 568
Scott, E. R., & Bottke, W. F. 2011, Impact Histories of Angrites, Eucrites, and Their Parent Bodies, M&PS, 46, 1878
Sharp, Z. C., McCubbin, F. M., & Shearer, C. K. 2013, A Hydrogen-based Oxidation Mechanism Relevant to Planetary Formation, E&PSL, 380, 88
Steenstra, E. S., Knibbe, J. S., Rai, N., & van Westrenen, W. 2016, Constraints on Core Formation in Vesta from Metal–Silicate Partitioning of Siderophile Elements, GeCoA, 177, 48
Steenstra, E. S., Sitabi, A. B., Lin, Y. H., et al. 2017, The Effect of Melt Composition on Metal–Silicate Partitioning of Siderophile Elements and Constraints on Core Formation in the Angrite Parent Body, GeCoA, 212, 62

Sun, C., & Yao, L. 2024, Redox Equilibria of Iron in Low- to High-Silica Melts: A Simple Model and its Applications to C-H-O-S Degassing, E&PSL, 638, 118742
Tissot, F. L. H., Collinet, M., Namur, O., & Grove, T. L. 2022, The Case for the Angrite Parent Body as the Archetypal First-generation Planetesimal: Large, Reduced and Mg-enriched, GeCoA, 338, 278
Touboul, M., Sprung, P., Aciego, S. M., Bourdon, B., & Kleine, T. 2015, Hf–W Chronology of the Eucrite Parent Body, GeCoA, 156, 106
Wade, J., & Wood, B. J. 2005, Core Formation and the Oxidation State of the Earth, E&PSL, 236, 78
Wadhwa, M. 2008, Redox Conditions on Small Bodies, the Moon and Mars, RvMG, 68, 493
Wasson, J. T., & Kallemeyn, G. W. 1988, Compositions of Chondrites, RSPTA, 325, 535
Weber, R. C., Lin, P.-Y., Garnero, E. J., Williams, Q., & Lognonné, P. 2011, Seismic Detection of the Lunar Core, Sci, 331, 309
Weiss, B. P., Berdahl, J. S., Elkins-Tanton, L., et al. 2008, Magnetism on the Angrite Parent Body and the Early Differentiation of Planetesimals, Sci, 322, 713
Woodland, A. B., Kornprobst, J., & Tabit, A. 2006, Ferric Iron in Orogenic Lherzolite Massifs and Controls of Oxygen Fugacity in the Upper Mantle, Litho, 89, 222
Xian, H., Zhu, J., Yang, Y., et al. 2023, Ubiquitous and Progressively Increasing Ferric Iron Content on the Lunar Surfaces Revealed by the Chang'e-5 Sample, NatAs, 7, 280
Zhang, H. L., Hirschmann, M. M., Lord, O. T., et al. 2024a, Ferric Iron Stabilization at Deep Magma Ocean Conditions, SciA, 10, eadp1752
Zhang, H., Yang, W., Zhang, D., et al. 2024b, Long-term Reduced Lunar Mantle Revealed by Chang'e-5 Basalt, NatCo, 15, 8328
Zhu, M.-H., Morbidelli, A., Neumann, W., et al. 2021, Common Feedstocks of Late Accretion for the Terrestrial Planets, NatAs, 5, 1286